Journal of Zhejiang University-SCIENCE A 2025 26(11):1114-1126
www.jzus.zju.edu.cn; www.springer.com/journal/11582
E-mail: jzus_a@zju.edu.cn

Research Article
https://doi.org/10.1631/jzus.A2400520

Numerical investigation of the detonation wave characteristics of boron-based gel propellant

He YANG, Liya HUANG✉, Jiarui ZHANG✉, Kun LIANG, Mingquan GONG

College of Aerospace Science and Engineering, National University of Defense Technology, Changsha 410073, China

Abstract: In this study, we aimed to investigate the detonation wave characteristics of a gel propellant with high boron content. A steady-state detonation wave model of a boron-based gel propellant considering the latent heat of phase change was proposed. The detonation wave model was validated through a comparative analysis with shock tube experiments, which revealed that the maximum deviation in the calculated peak detonation pressure was 8% based on various initial pressures. Upon iterative calculations, the eigenvalue detonation velocity of the boron-based gel propellant under default working conditions was obtained as 1831.5 m/s. Subsequently, the refined model was used to study the structure and characteristics of the detonation wave flow field. The effects of incoming flow conditions, fuel parameters, and initial operating state on the detonation wave flow field of the propellant were investigated numerically. The findings revealed that stable and self-sustaining propagation of the detonation wave can be achieved only when its propagation velocity matches the eigenvalue detonation velocity. Note that an increase in initial temperature resulted in elevated gas phase temperature, density, detonation pressure, and particle phase temperature. An increase in boron content within the gel propellant increased the gas phase temperature but decreased the gas phase density and detonation pressure. At the Chapman-Jouguet (CJ) plane, the gas phase temperature and density, along with the particle phase temperature and detonation pressure, reached their peak values when the oxidizer reacted with the propellant in accordance with the stoichiometric ratio.

Key words: Boron-based gel propellant; Detonation flow field; Polyphase detonation; Detonation wave characteristics

1 Introduction

With the rapid development of the aerospace field, the requirements for propulsion performance of various types of aircraft are increasing (Liu et al., 2023). As a promising combustion organization mode, detonation has great potential in the field of high-performance propulsion due to its advantages of a faster energy release rate and higher thermal cycle efficiency (Wang et al., 2009; Fan et al., 2022; Shen et al., 2022). In terms of fuel development, gel propellant is a new type of energetic material that uses gelling agents to gel liquid propellants and can maintain long-term stability (von Kampen et al., 2007; Yang et al., 2018; Huang et al., 2024). Adding energetic solid additives such as boron powder into a gel propellant can significantly improve its energy density (Duan et al., 2023; Glushkov et al., 2023). Hence, the use of gel fuel for detonation combustion presents a highly promising blueprint for future aircraft propulsion systems. Currently, most research in the field of detonation centers on gas (Miao et al., 2019; Han et al., 2022; Rojas Chavez et al., 2023) or liquid (Fan et al., 2021; Meng et al., 2022; Wang and Weng, 2022) fuel, yet the use of gel propellants in this field holds immense potential.

A gel propellant combines the advantages of solid and liquid propellants, making its application in various propulsion systems promising; therefore, it has been widely studied by scholars (Padwal et al., 2021). Nachmoni and Natan (2000) carried out experiments to study the combustion characteristics of gel propellant and found that it is more difficult to ignite than liquid propellant, and high pressure can improve this ignition performance. To enhance fuel energy density and combustion performance, researchers have been working on adding metal fuel additives into gel propellants

✉ Liya HUANG, huangliya05@nudt.edu.cn
Jiarui ZHANG, zhangjiarui@nudt.edu.cn
Liya HUANG, https://orcid.org/0009-0003-3177-5810

Received Nov. 8, 2024; Revision accepted Mar. 24, 2025;
Crosschecked Oct. 11, 2025; Online first Nov. 19, 2025

for many years (von Kampen et al., 2007; Jin et al., 2022). Chen and Zhang (2011) pointed out that boron and aluminum are ideal energetic materials based on safety, density, combustion products, and other factors. Küçükosman et al. (2023) used a high-speed camera and a thermal imager to study the combustion characteristics of a gel propellant with boron-based particles added. The results showed that the addition of boron-based particles could shorten the ignition delay time of the propellant. To address the challenging issues of atomization and combustion, Hu and Weng (2011, 2016) studied the detonation process of an aluminum-based gel propellant, which showed that the high-intensity turbulence and shock waves generated during detonation have the potential to significantly overcome these difficulties. Besides, they found that the addition of aluminum powder can reduce the initial ignition energy requirement of a gel propellant. Palaszewski et al. (2004) also verified the advantages of detonation of the aluminum-based gel propellant through engine experiments.

Due to the characteristics of high temperature, high pressure, and supersonic velocity of a detonation wave, the data that can be measured in an experiment are limited. As an alternative approach, numerical simulations can be used to study detonation waves, providing valuable insights into the internal flow field (Liang and Wang, 2019; Lei et al., 2020; Sun et al., 2023; Liu et al., 2024). Schumaker et al. (2021) used the Zeldovich-von Neumann-Döring (ZND) model to predict the cell size of methane-oxygen detonation under different pre-detonation pressures, and the results were consistent with those of tests. Lu et al. (2021) used the ZND model to calibrate a chemical-diffusive model and obtained the same cell structure as in a hydrogen detonation test. Unlike traditional gas detonation, multiphase detonation has complex mass, momentum, and energy exchange processes between the dispersed phase and the gas phase, and relevant numerical simulation studies tend to be simplified (Shao et al., 2010; Liu et al., 2020). Salvadori et al. (2023) used a sparse model to study the reaction process of kerosene, hydrogen, and air in a rotating detonation engine, and obtained a stable detonation wave structure in a 3D flow field. Moreover, they found that the addition of hydrogen contributes to liquid phase evaporation and combustion. Hong et al. (2009) simulated the detonation wave of a mixture of explosives and aluminum particles, and concluded that the addition of aluminum particles can improve the velocity, pressure, and temperature of a detonation wave.

Boron has a higher caloric value than aluminum (Pang et al., 2022). However, achieving efficient combustion in the heterogeneous chemical reaction process of a boron-based gel propellant poses an inherent challenge, and research into its detonation process has been scarce. Specifically, numerical simulations of the detonation process of boron-based gel propellants have not been reported publicly, and the structure and characteristics of their detonation waves remain unclear. Therefore, in this study, we established a 1D steady-state model of a boron-based gel propellant detonation wave based on the ZND model, and the reliability of the model was verified by ground tests. The effects of flow conditions, propellant parameters, and the initial operating state on the detonation wave structure and propagation process of the propellant were studied by numerical simulation. The results provide theoretical support for the application of boron-based gel propellants to detonation.

2 Numerical modeling

2.1 Physical model

The ZND model is a theoretical model describing the structure of a detonation wave. It assumes that the detonation wave consists of a leading shock wave followed by a combustion reaction zone. Based on the ZND model, a 1D steady-state detonation wave structure of a gel propellant with the coordinate system fixed on the leading shock wave front is depicted in Fig. 1, where ρ_g, u_g, and T_g respectively denote the density, velocity, and temperature of the gas phase, ρ_p, u_p, and T_p respectively denote the density, velocity, and temperature of the particle phase, P denotes the pressure of the mixture, u denotes the velocity of the mixture, and the subscripts 0 and 1 denote reactant and product states, respectively. After passing through the leading shock wave, the temperature of the gas phase reactants goes through an adiabatic compression process, and the gel components are vaporized and burned in a very short time through heat transfer between the two phases in the induction region. At the same time, the temperature of the boron particles rises and the oxide layer on the surface of the particles gradually decreases

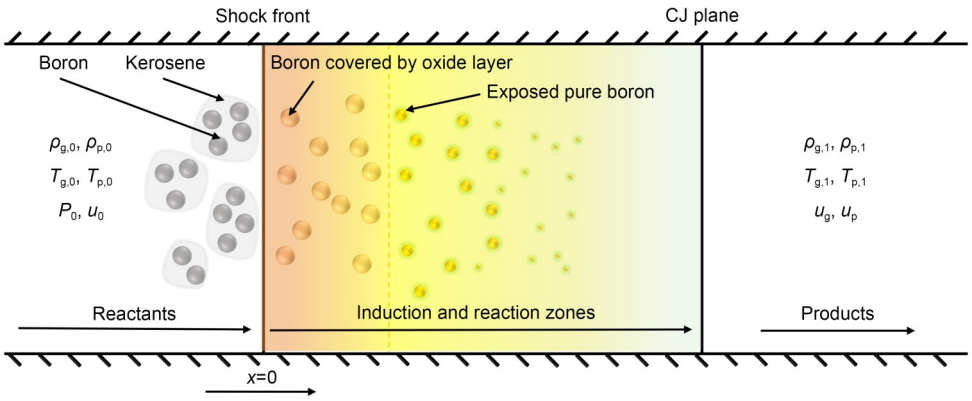

Fig. 1 Schematic diagram of 1D steady-state detonation wave structure

until the ignition temperature (978 K) (Zhou et al., 2015) is reached. In the reaction zone, the exposed pure boron particles react heterogeneously and release their chemical energy. The gas phase material expands and accelerates away from the leading shock wave, while the reverse thrust generated by the expansion maintains the propagation of the leading shock wave. Until the gas phase material accelerates to the local sound velocity relative to the leading shock wave, the change of the downstream flow field will no longer affect the upstream flow field, and the gas phase expansion behind the sonic plane will no longer contribute to maintaining the propagation of the detonation wave. Here, the sonic plane is also called the Chapman-Jouguet (CJ) plane.

The detonation process of a gel propellant with boron particles added is relatively complicated. To facilitate calculation, the following simplified assumptions were first made:

(1) All particles are spherical, the same size, uniformly distributed in the gas phase, and fill the entire space. Interactions between particles are ignored.

(2) Aviation kerosene has a low ignition point and reacts rapidly compared to boron particles (Foelsche et al., 1999; Sun et al., 2008; Li et al., 2009, 2011). Therefore, it is assumed that the kerosene component first completes combustion after the leading shock wave, and then the boron particles react.

(3) The reaction rate of boron particles with oxygen is much higher than that of other substances in the gas phase, and the duration of the actual detonation process is very short. Therefore, it is assumed that the particle phase reacts only with oxygen in the environment.

(4) It is assumed that the Biot number of boron particles is extremely small, the thermal conductivity of particles is excellent, and the temperature inside the particles is always evenly distributed.

(5) The reaction product (B_2O_3) is regarded as a gas phase component, and the latent heat of phase transition is included in the internal energy.

2.2 Governing equations

Based on the above assumptions, kerosene burns rapidly after the leading shock wave, which serves as the boundary condition for the detonation wave flow field calculation. Within the detonation wave flow field, the reaction process of boron is mainly considered. For the 1D steady-state reaction process of the two-phase mixture, the mass conservation equation, momentum conservation equation, and energy conservation equation are separated. Specifically, for the gas phase,

$$\frac{\mathrm{d}}{\mathrm{d}x}(\rho_\mathrm{g}u_\mathrm{g})=S_\mathrm{d}, \tag{1}$$

$$\frac{\mathrm{d}}{\mathrm{d}x}(\rho_\mathrm{g}u_\mathrm{g}^2+P)=-F_\mathrm{d}+S_\mathrm{d}u_\mathrm{p}, \tag{2}$$

$$\begin{aligned}\frac{\mathrm{d}}{\mathrm{d}x}\left[\rho_\mathrm{g}u_\mathrm{g}\left(e_\mathrm{g}+\frac{u_\mathrm{g}^2}{2}+\frac{P}{\rho_\mathrm{g}}\right)\right]=\\ -Q_\mathrm{d}-F_\mathrm{d}u_\mathrm{p}+S_\mathrm{d}\left(e_\mathrm{p}+\frac{u_\mathrm{p}^2}{2}+q_\mathrm{c}\right),\end{aligned} \tag{3}$$

$$\frac{\mathrm{d}}{\mathrm{d}x}(\rho_i u_\mathrm{g})=S_i,\quad i=\mathrm{O_2},\ \mathrm{B_2O_3},\ \mathrm{N_2},\ \mathrm{CO_2},\ \mathrm{H_2O}, \tag{4}$$

and similarly, for the particle phase,

$$\frac{\mathrm{d}}{\mathrm{d}x}(\rho_\mathrm{p}u_\mathrm{p})=-S_\mathrm{d}, \tag{5}$$

$$\frac{\mathrm{d}}{\mathrm{d}x}(\rho_\mathrm{p}u_\mathrm{p}^2)=F_\mathrm{d}-S_\mathrm{d}u_\mathrm{p}, \tag{6}$$

$$\frac{\mathrm{d}}{\mathrm{d}x}\left[\rho_{\mathrm{p}}u_{\mathrm{p}}\left(e_{\mathrm{p}}+\frac{u_{\mathrm{p}}^2}{2}\right)\right]=Q_{\mathrm{d}}+F_{\mathrm{d}}u_{\mathrm{p}}-S_{\mathrm{d}}\left(e_{\mathrm{p}}+\frac{u_{\mathrm{p}}^2}{2}\right), \quad (7)$$

where e_{g} denotes the internal energy of the gas phase, e_{p} denotes the internal energy of the particle phase, ρ_i denotes the density of species i and S_i denotes its mass transfer rate in unit volume, q_{c} denotes the calorific value of boron, S_{d} denotes the interphase mass transfer rate in unit volume, F_{d} denotes the interphase force transfer in unit volume, and Q_{d} denotes the interphase heat transfer rate in unit volume.

A schematic diagram of the ignition process of boron particles is shown on the left side of Fig. 2. In the ignition stage, the oxide layer on the surface of the boron particles melts first after reaching the melting point (723 K), and oxygen diffuses through the oxide layer to the boron surface for reaction, generating boron oxide and releasing heat. At the same time, boron oxide evaporates on the surface of the particles. When the consumption rate of boron oxide is higher than its generation rate, the liquid oxide layer thins gradually, and the boron particle ignition stage is considered to be concluded after complete consumption of the oxide layer (King, 1972). The mass conversion rate of boron particles per unit volume in the ignition stage can be expressed as:

$$S_{\mathrm{d}}=nR_{\mathrm{B}}M_{\mathrm{W,B}}, \quad (8)$$

$$R_{\mathrm{B}}=64.8\times10^{-8}\cdot r_{\mathrm{p}}^2T_{\mathrm{p}}\mathrm{e}^{-22600/T_{\mathrm{p}}}P_{\mathrm{O_2}}/x, \quad (9)$$

where $M_{\mathrm{W,B}}$ denotes the atomic weight of boron, R_{B} denotes the consumption rate of boron, r_{p} denotes the particle size, $P_{\mathrm{O_2}}$ denotes the partial pressure of oxygen, x denotes the thickness of the oxide layer, and n denotes the number of boron particles per unit volume, which can be expressed as:

$$n=n_0u_{\mathrm{p},0}/u_{\mathrm{p}}, \quad (10)$$

$$n_0=\frac{3\rho_{\mathrm{p},0}}{4\pi r_{\mathrm{p},0}^3\rho_{\mathrm{B}}}, \quad (11)$$

where n_0 denotes the initial number of boron particles per unit volume, $u_{\mathrm{p},0}$ denotes the initial velocity of the particle phase, $r_{\mathrm{p},0}$ denotes the initial particle size of the boron particles, and ρ_{B} denotes the density of boron.

After the oxide layer on the surface of the particles is exhausted, the boron particles react violently with the surrounding oxidizing atmosphere directly, releasing a lot of heat. Due to the high boiling point of boron particles, scholars believe that the combustion process of boron particles is mainly surface combustion, and they have used the overall reaction to describe the boron combustion process (Glushkov et al., 2023). As shown on the right side of Fig. 2, the intermediate gas phase product formed by surface combustion will diffuse into the environment and react quickly to generate boron oxide (Yuan et al., 2021). The combustion rate of boron particles is affected by the diffusion rate of the components and the chemical kinetic rate of the combustion reaction. The dominance of surface reactions in controlling the particle combustion process is determined through the Damköhler number (*Da*). When $Da>1$, the particle combustion rate is controlled by the diffusion rate, when $Da<1$, it is controlled by the surface reaction kinetic rate, and when $Da=1$, the combustion is simultaneously controlled by both chemical kinetics and diffusion.

Under the condition of diffusion control, the boron combustion process is affected by the diffusion rate of oxygen on the surface of the particles. According to diffusion combustion theory, the mass conversion rate of boron particles per unit volume can be expressed as:

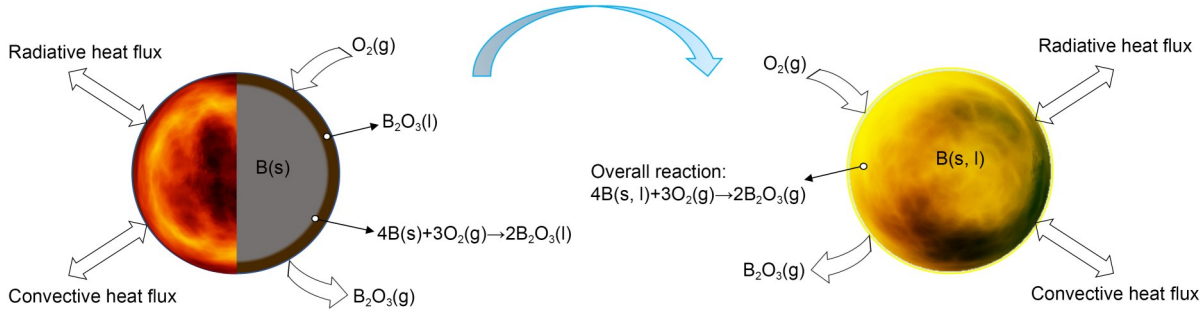

Fig. 2 Schematic diagram of boron particle ignition and combustion model

$$S_{\mathrm{d}}=4n\pi r_{\mathrm{p}}\rho_{\mathrm{g}}D_{\mathrm{O}_2}\ln\left(\beta Y_{\mathrm{O}_{2,\infty}}+1\right), \tag{12}$$

where D_{O_2} denotes the diffusion coefficient of oxygen in the mixed gas, β denotes the mass ratio of the reactants in the surface total inclusion reaction, and $Y_{\mathrm{O}_{2,\infty}}$ denotes the mass fraction of oxygen in the environment.

Under the conditions controlled by the chemical kinetic mechanism of the combustion reaction, the mass conversion rate of boron particles per unit volume can be expressed as:

$$S_{\mathrm{d}}=4n\pi r_{\mathrm{p}}^2M_{W,\mathrm{B}}kPX_{\mathrm{O}_{2,\infty}}, \tag{13}$$

where $X_{\mathrm{O}_{2,\infty}}$ denotes the mole fraction of oxygen in the ambient atmosphere, and k denotes the reaction rate coefficient, obtained by Li and Williams (1991) through experiments, which can be expressed as:

$$k=\begin{cases}0.0625\pm0.0125, & T_{\mathrm{p}}>2400\ \mathrm{K},\\ \dfrac{31.5}{\sqrt{T_{\mathrm{p}}}}\times\exp\left(\dfrac{-5630}{T_{\mathrm{p}}}\right), & 1750\ \mathrm{K}<T_{\mathrm{p}}\leqslant2400\ \mathrm{K},\\ \dfrac{1.57\times10^8}{\sqrt{T_{\mathrm{p}}}}\times\exp\left(\dfrac{-32500}{T_{\mathrm{p}}}\right), & 1600\ \mathrm{K}<T_{\mathrm{p}}\leqslant1750\ \mathrm{K}.\end{cases} \tag{14}$$

According to the above hypothesis, the particle phase is uniformly dispersed in the gas phase, and the change of gas phase velocity will drive the particle phase to change together. In unit volume, the force of gas relative to the particle phase can be expressed as:

$$F_{\mathrm{d}}=\frac{n}{2}\pi r_{\mathrm{p}}^2C_{\mathrm{D}}\rho_{\mathrm{g}}|u_{\mathrm{g}}-u_{\mathrm{p}}|(u_{\mathrm{g}}-u_{\mathrm{p}}), \tag{15}$$

$$C_{\mathrm{D}}=\begin{cases}\dfrac{24}{Re(1+Re^{2/3}/6)}, & Re<1000,\\ 0.424, & Re\geqslant1000,\end{cases} \tag{16}$$

where C_{D} is the drag coefficient, Re is the Renolds number of the two phases, which can be expressed as:

$$Re=2\rho_{\mathrm{g}}r_{\mathrm{p}}|u_{\mathrm{g}}-u_{\mathrm{p}}|/\mu_{\mathrm{g}}, \tag{17}$$

where μ_{g} denotes the gas phase viscosity coefficient. After the leading shock wave, the temperature of the gas phase increases rapidly, resulting in a significant temperature difference between the gas phase and the particle phase. Consequently, heat transfer processes commence between the two phases. In unit volume, the interphase heat transfer rate can be expressed as:

$$Q_{\mathrm{d}}=2n\pi r_{\mathrm{p}}\lambda_{\mathrm{g}}Nu(T_{\mathrm{g}}-T_{\mathrm{p}}), \tag{18}$$

where λ_{g} denotes the gas phase thermal conductivity, and Nu denotes the Nusselt number, which can be expressed empirically as:

$$Nu=2+0.6Re^{0.5}Pr^{0.33}, \tag{19}$$

where Pr denotes the Prandtl number.

According to the above hypothesis, the latent heat associated with phase transitions is incorporated within the internal energy, and the interrelation between the temperatures of the gas phase and the particle phase, as well as the internal energy, can be expressed as:

$$T_{\mathrm{g}}=\begin{cases}e_{\mathrm{g}}/c_{\mathrm{v,g}}, & e_{\mathrm{g}}<e_{\mathrm{g,f(s)}},\\ T_{\mathrm{B_2O_3,f}}, & e_{\mathrm{g,f(s)}}\leqslant e_{\mathrm{g}}\leqslant e_{\mathrm{g,f(l)}},\\ (e_{\mathrm{g}}-e_{\mathrm{g,f(l)}})/c_{\mathrm{v,g}}+T_{\mathrm{B_2O_3,f}}, & e_{\mathrm{g,f(l)}}<e_{\mathrm{g}}<e_{\mathrm{g,b(l)}},\\ T_{\mathrm{B_2O_3,b}}, & e_{\mathrm{g,b(l)}}\leqslant e_{\mathrm{g}}\leqslant e_{\mathrm{g,b(g)}},\\ (e_{\mathrm{g}}-e_{\mathrm{g,b(g)}})/c_{\mathrm{v,g}}+T_{\mathrm{B_2O_3,b}}, & e_{\mathrm{g}}>e_{\mathrm{g,b(g)}},\end{cases} \tag{20}$$

$$T_{\mathrm{p}}=\begin{cases}e_{\mathrm{p}}/c_{\mathrm{p(s)}}, & e_{\mathrm{p}}<e_{\mathrm{p,f(s)}},\\ T_{\mathrm{B,f}}, & e_{\mathrm{p,f(s)}}\leqslant e_{\mathrm{p}}\leqslant e_{\mathrm{p,f(l)}},\\ (e_{\mathrm{p}}-e_{\mathrm{p,f(l)}})/c_{\mathrm{p(l)}}+T_{\mathrm{B,f}}, & e_{\mathrm{p,f(l)}}<e_{\mathrm{p}}<e_{\mathrm{p,b(l)}},\\ T_{\mathrm{B,b}}, & e_{\mathrm{p}}\geqslant e_{\mathrm{p,b(l)}},\end{cases} \tag{21}$$

where $e_{\mathrm{g,f(s)}}$ and $e_{\mathrm{g,f(l)}}$ respectively denote the specific internal energy of the gas phase corresponding to boron oxide being entirely in its solid state and liquid state when the temperature reaches the melting point of boron oxide, $e_{\mathrm{g,b(l)}}$ and $e_{\mathrm{g,b(g)}}$ respectively denote the specific internal energy of the gas phase corresponding to boron oxide being entirely in its liquid state and gas state when the temperature reaches the boiling point of boron oxide, $e_{\mathrm{p,f(s)}}$ and $e_{\mathrm{p,f(l)}}$ respectively denote the specific internal energy of the particle phase corresponding to boron particle being entirely in its solid state and liquid state when the temperature reaches the melting point of boron, $e_{\mathrm{p,b(l)}}$ denotes the specific internal energy of the particle phase corresponding to

the boron particles being entirely in their liquid state when the temperature reaches the boiling point of boron, $c_{v,g}$ denotes the specific heat capacity at constant volume for the gas phase, $c_{p(s)}$ and $c_{p(l)}$ respectively denote the specific heat capacity of the particle phase in solid state and liquid state, $T_{B_2O_3,f}$ and $T_{B_2O_3,b}$ respectively denote the melting point temperature and boiling point temperature of the boron oxide, and $T_{B,f}$ and $T_{B,b}$ respectively represent the melting point temperature and boiling point temperature of the boron particle.

2.3 Numerical set up

As shown in Fig. 1, the disturbance behind the CJ surface no longer affects the leading shock wave, and the region between the leading shock wave surface and the CJ surface was set as the solution domain in this study. For the region where x<0, the initial reaction parameters are given artificially. At x=0, the von Neumann state parameters of the gas phase after the leading shock were obtained according to the Rankin-Hugoniot relation. Since the inertia of the particle phase is large, we assumed that the state parameters remain unchanged after passing the leading shock wave. Unless otherwise specified, the default gas phase flow and propellant temperatures were 300 K, the initial pressure was 0.2 MPa, the boron content in the gel propellant was 40%, the boron particle size was 2 μm, and the oxidant and propellant were provided according to the stoichiometric ratio. The 4th-order Runge-Kutta method was used to solve the conservation equation in the solution domain.

The ordinary differential equation of gas phase velocity can be obtained by combining the conservation equations, as shown in Eq. (22), where the value of Φ is related to the degree of reaction, and Ma is the Mach number. Therefore, the eigenvalue detonation velocity can be obtained by using the regularity condition as the criterion.

$$\frac{\mathrm{d}u_g}{\mathrm{d}x}=\frac{\Phi}{1-Ma^2}. \tag{22}$$

Suppose that an arbitrary leading shock wave velocity is calculated to obtain the von Neumann state parameter, and then the ZND structure of the detonation wave is obtained by integration. With the advance of integration, the denominator in the above formula gradually vanishes, but the corresponding numerator does not necessarily vanish at the same time for the arbitrarily selected detonation velocity, so the eigenvalue detonation velocity that satisfies the regularity condition at the sonic singularity can be obtained by iterative calculation.

2.4 Model validation

To verify the accuracy of this model, we carried out grid independence verification. An arbitrary leading shock wave velocity was assumed, and after iterative calculation by Eq. (22), the eigenvalue detonation velocity was 1831.5 m/s. The incoming velocity was set as the eigenvalue detonation wave velocity, and three sizes of grids (1, 0.1, and 0.01 mm) were used for calculation, respectively. The pressure distribution of the boron-based gel propellant detonation wave flow field was obtained, as shown in Fig. 3.

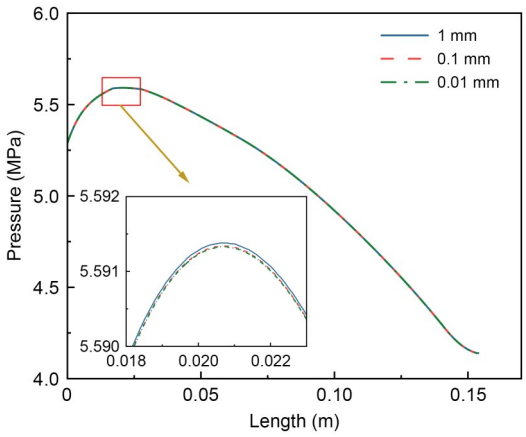

Fig. 3 Pressure distribution of detonation wave with different mesh sizes

Fig. 3 shows that the change of mesh size has little influence on the calculation results. According to the local magnification diagram, the peak value of detonation pressure increases slightly with increasing mesh size, but there is no significant difference in the overall calculation results. Therefore, in subsequent research, the 0.1 mm mesh size was used for calculation.

Experimental validation was also carried out, in which a gel propellant with 40% boron content was prepared and then tested in a detonation tube. The initiation of detonation of boron-based gel propellants was induced mainly by igniting an H_2/O_2 mixture, and the initial pressure in the detonation tube was adjusted by controlling the duration of the supply of the premixed gas. Six high-frequency dynamic transducers

were set on the wall of the detonation tube, and the initial pressures before detonation in three tests were measured to be 0.17, 0.19, and 0.22 MPa, respectively. Detailed information on this experimental setup is given by Liang et al. (2024). In parallel, we used a gel propellant with 40% boron content to conduct numerical simulations under the same initial conditions as in the experiments. In these simulations, we set the average diameter of the boron particles to 2 μm and the initial temperature to 300 K. The resulting peak detonation wave pressures across different initial pressure conditions were obtained and compared with experimental data measured by high-frequency dynamic transducers (Fig. 4).

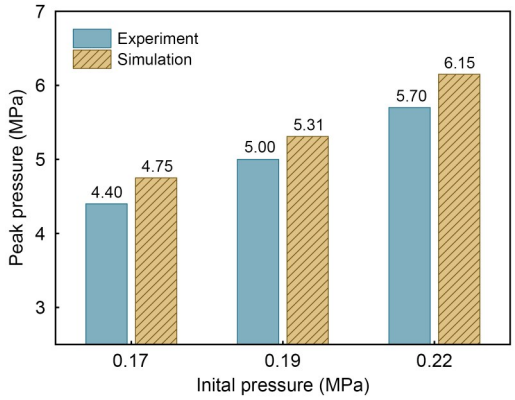

Fig. 4 Comparison between the experiment and simulation values of the detonation wave peak pressure under different initial pressures

Fig. 4 shows that the errors of the detonation wave peak pressure in the three tests compared with the simulated values were 8.0%, 6.2%, and 7.9%, respectively. The efficacy of the simulation was further confirmed by the consistency between the experiment and simulation, which supports the use of the simulation method to investigate the flow field structure of detonation waves.

3 Results and discussion

3.1 Flow field structure analysis

The numerical model verified by experiments was adopted to carry out the calculation under default working conditions, and the incoming flow velocity was set as the eigenvalue detonation velocity of 1831.5 m/s. The distribution of the gas phase and particle phase densities, velocities, and temperatures, oxidation product density, and detonation pressure in the detonation wave flow field were obtained (Fig. 5).

As shown in Figs. 5a and 5b, the reactant reaches the von Neumann state after passing through the leading shock wave, the density and temperature of the gas phase rise sharply, and then the particle phase temperature increases under the action of interphase heat transfer. In the induction zone, boron particles are covered by an oxide layer, leading to a lower reaction rate. Until the oxide layer is exhausted, the boron particles enter the combustion stage, quickly reacting to release a lot of heat, leading to a rapid increase in gas phase and particle phase temperature. The heated gas expands and accelerates away from the leading shock wave, resulting in a decrease in the gas phase density and detonation wave pressure, as shown in Figs. 5a and 5c. Due to the consideration of the latent heat in the phase transition process in the present model, the temperature of the particle phase remains unchanged when it reaches the melting point of boron. As the reaction progresses, the particle size diminishes, resulting in a decrease in the reaction rate, which subsequently causes a gradual reduction in the heating rates of both the gas and particle phases, as well as the generation rate of oxidation products in the latter half of the flow field. Note that the temperature of the particle phase exceeds the boiling point of boron (4200 K) under atmospheric pressure during its combustion process, which is due to the extremely high pressure in the detonation environment. According to the Clausius-Clapeyron equation, the boiling point of a substance increases with an increase of pressure. In addition, there is a large velocity difference between the gas phase and the particle phase after the leading shock wave, as shown in Fig. 5d, which then tends to equalize under the action of the drag force.

3.2 Influence of incoming flow conditions

In this subsection, 0.9, 1.0, and 1.1 times the eigenvalue detonation velocity are taken as the incoming flow velocity to carry out the calculation and analysis, and the corresponding detonation wave structures are obtained. The distributions of Φ and $1-Ma^2$ in Eq. (22) are shown in Fig. 6.

As shown in Fig. 6, when the incoming flow velocity is equal to the eigenvalue detonation velocity, Φ vanishes at the point where $1-Ma^2$ approaches zero,

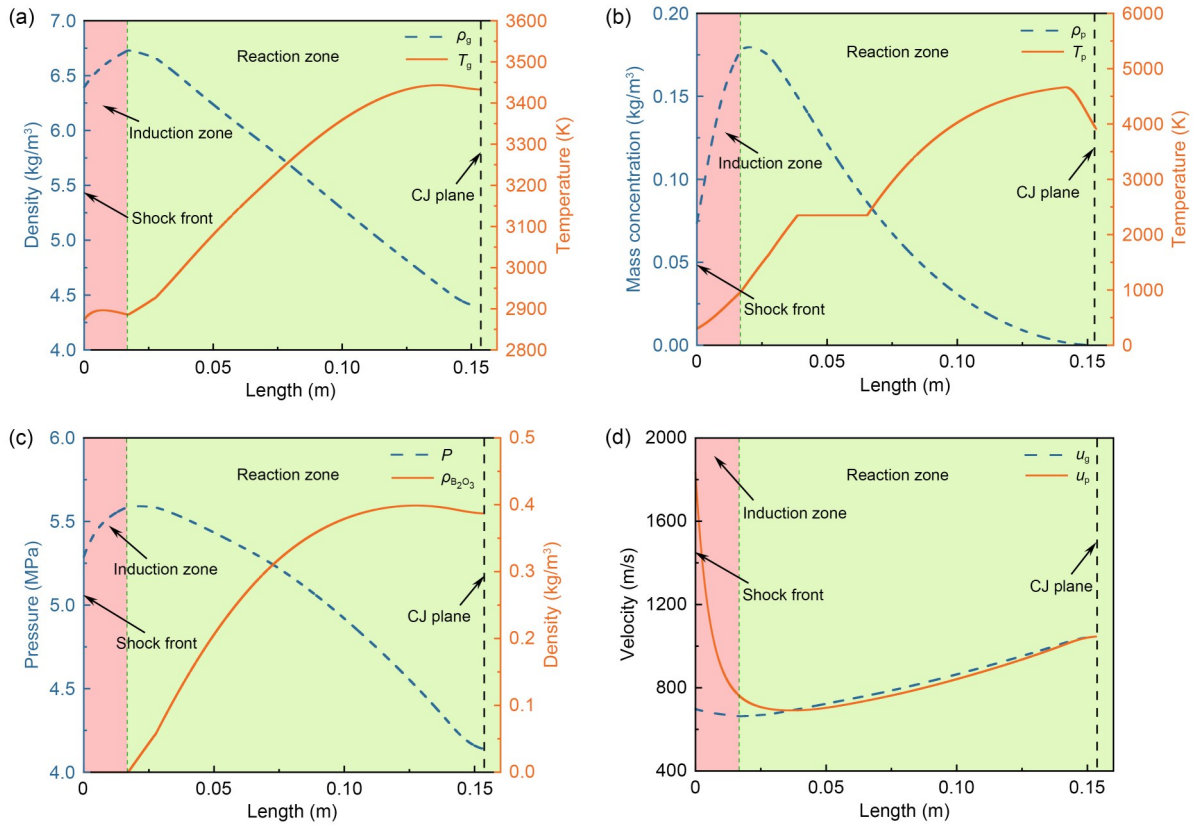

Fig. 5 Flow field structure of detonation wave using gel propellant: (a) gas phase density (ρ_g) and temperature (T_g); (b) particle phase mass concentration (ρ_p) and temperature (T_p); (c) detonation pressure (P) and oxidation product density ($\rho_{B_2O_3}$); (d) gas phase velocity (u_g) and particle phase velocity (u_p)

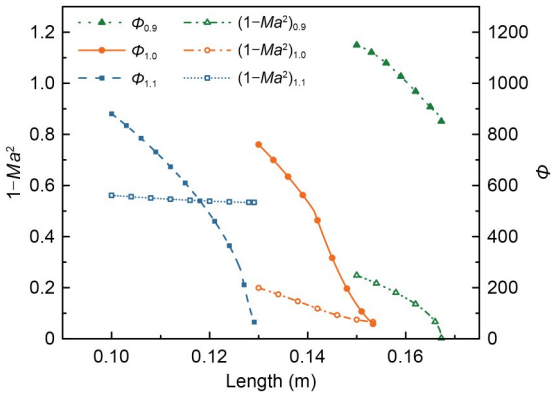

Fig. 6 Distribution of $1-Ma^2$ and Φ under different incoming flow velocities (0.9, 1.0, and 1.1 times the eigenvalue detonation velocity)

satisfying the regularity condition. As a result, the detonation wave can propagate stably. When the incoming flow velocity is greater than the eigenvalue detonation velocity, the $1-Ma^2$ is greater than zero when Φ approaches zero, which indicates that the chemical reaction in the detonation wave is complete before the gas phase accelerates to the speed of sound (u_{sound}), and the flow field behind the leading shock wave is entirely subsonic. As a result, the disruption to the downstream flow field can traverse the reaction zone, thereby diminishing the intensity of detonation. Moreover, the detonation wave cannot propagate in a stable manner without the intervention of external forces, ultimately leading to an overdriven detonation. In addition, when the incoming flow velocity is less than the eigenvalue detonation velocity, Φ is greater than zero at the point where $1-Ma^2$ approaches zero, indicating that there is a singularity when the gas phase accelerates to the speed of sound, and the detonation wave cannot propagate stably at this time.

In the context of the practical application of boron-based gel propellant detonation, the total temperatures under Ma=2.3, Ma=2.5, and Ma=2.7 operating conditions, at a flight altitude of 10 km, are recorded as 459 K, 502 K, and 549 K, respectively. These temperatures serve as the initial temperatures for the incoming flow. With increasing initial temperature, the gas phase

temperature, particle phase temperature, gas phase density, and pressure of the detonation wave are increased, and the reaction speed is significantly accelerated. However, an excessive increase in reaction speed can trigger overdriven detonation. As shown in Fig. 7, the chemical reaction in the detonation wave is complete before the gas phase accelerates to the speed of sound, rendering the detonation wave unstable and impeding its consistent propagation. To obtain steadily propagating detonation waves, we calculated the characteristic detonation velocities under different inflow temperatures using the regularity condition, yielding values of 1195 m/s (459 K), 1094 m/s (502 K), and 1009 m/s (549 K). Additionally, we calculated the flow field parameters of the steadily propagating detonation wave under variable incoming flow temperatures (Fig. 8).

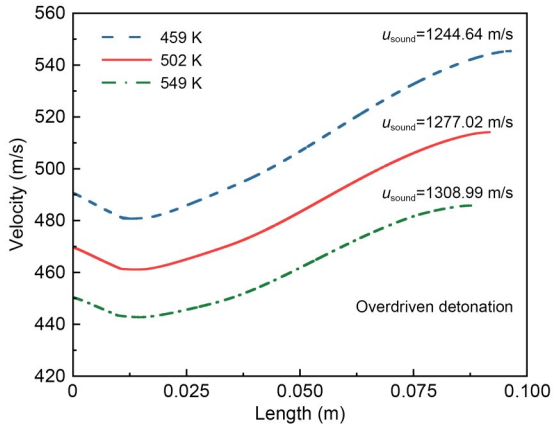

Fig. 7 Distribution of overdriven detonation wave gas velocities under different incoming temperatures

Fig. 8 shows that the gas phase temperature, particle phase temperature, gas phase density, and detonation pressure of the steadily propagating detonation wave all decrease with increasing incoming flow temperature. Due to the decrease of gas phase expansion capacity caused by the increase of incoming flow temperature, it is necessary to reduce the incoming flow velocity to avoid overdriven detonation. According to the Rankine-Hugoniot relationship, the gas phase parameters decrease after adiabatic compression of the leading shock wave, resulting in a decrease of the presented

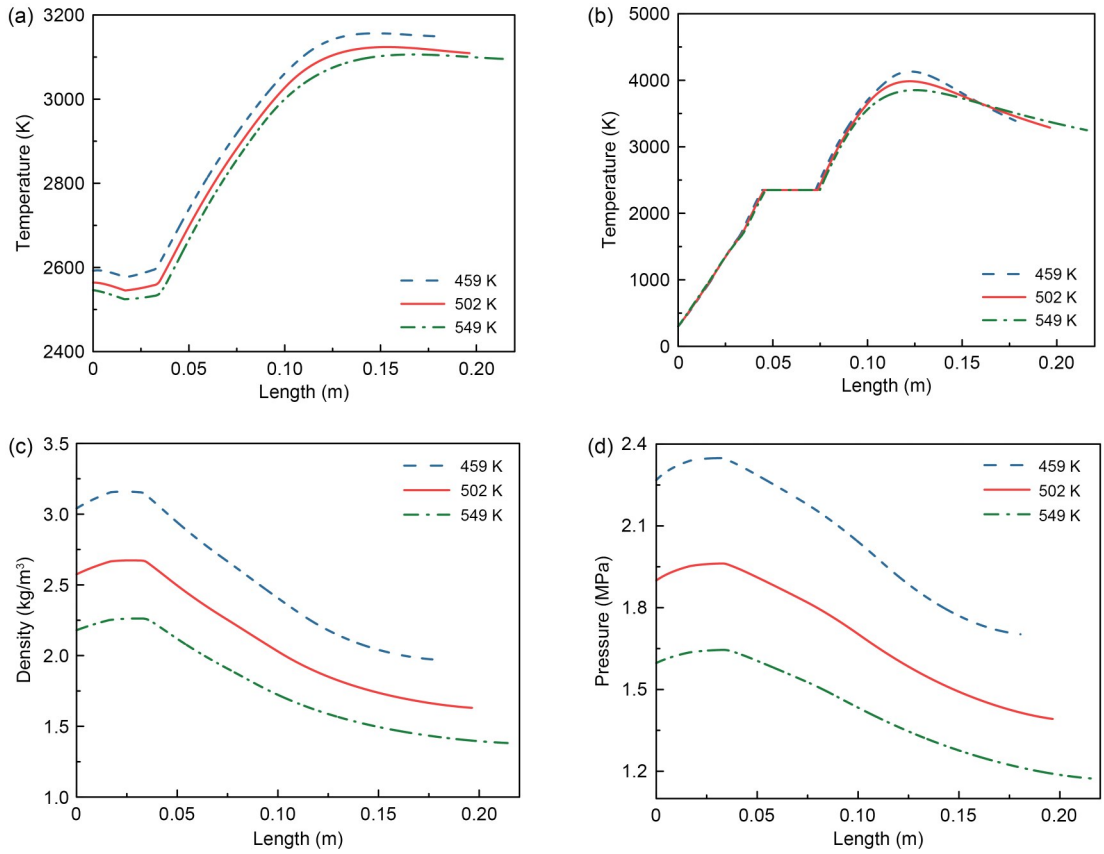

Fig. 8 Distribution of stable detonation wave flow field parameters under different incoming temperatures: (a) gas phase temperature; (b) particle phase temperature; (c) gas phase density; (d) detonation pressure

detonation wave flow field parameters of boron-based gel propellants.

3.3 Influence of propellant parameters

Under the default working condition, the content of boron particles in the gel propellant was set to 10%, 20%, 30%, and 40%, respectively, and the changes in the parameters of the detonation wave flow field were calculated (Fig. 9).

Fig. 9a shows the variation of gas phase temperature in the detonation wave of gel propellants with different boron contents. As the boron content in the gel propellant rises, the gas phase temperature observed following the leading shock wave diminishes. This is attributed to the kerosene in the propellant, which burns first and releases heat, with its content being the determining factor in establishing the initial gas phase temperature. As a result, the gas phase density and detonation pressure in the initial stage in Figs. 9c and 9d increase with the increase of boron content. Because the calorific value of boron is much higher than that of kerosene, the gas phase temperature in the latter part of the flow field increases with the increase of boron content. As can be seen from Fig. 9b, the particle phase temperature also increases with increasing boron content.

3.4 Influence of initial operating state

The stoichiometric air-fuel ratio of the chemical reaction of a boron-based gel propellant under the default working condition is about 12.6. The oxidizer and propellant were supplied according to the equivalence ratios (φ) of 0.8, 0.9, 1.0, and 1.1, respectively. The corresponding parameters of the detonation wave flow field are shown in Fig. 10.

As shown in Figs. 10b and 10d, the particle phase temperature and detonation pressure of the detonation wave flow field exhibit a trend of initially increasing and then decreasing with the increase of reaction equivalence ratio, reaching their peak values when the equivalence ratio is 1.0. This behavior can be attributed to complete reaction between the oxidant and propellant under the stoichiometric ratio, resulting in sufficient energy release without any excess materials to

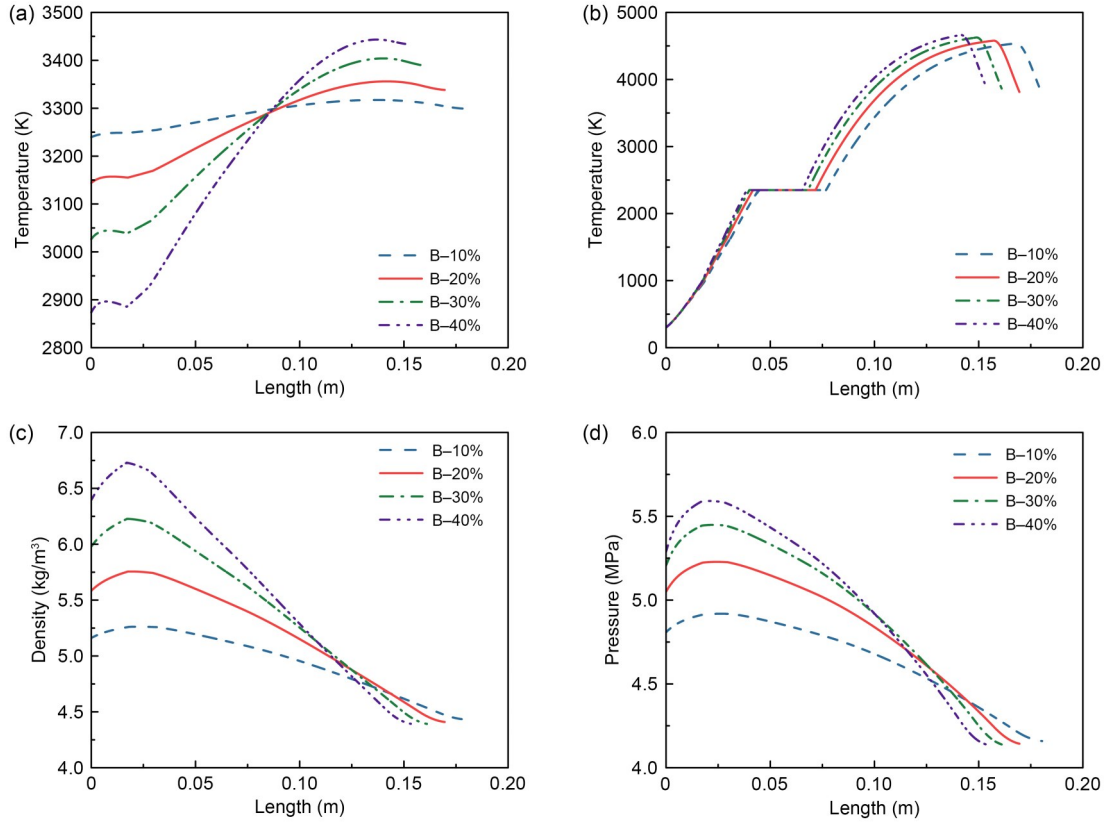

Fig. 9 Distribution of detonation wave flow field parameters under gel propellants with different boron contents: (a) gas phase temperature; (b) particle phase temperature; (c) gas phase density; (d) detonation pressure

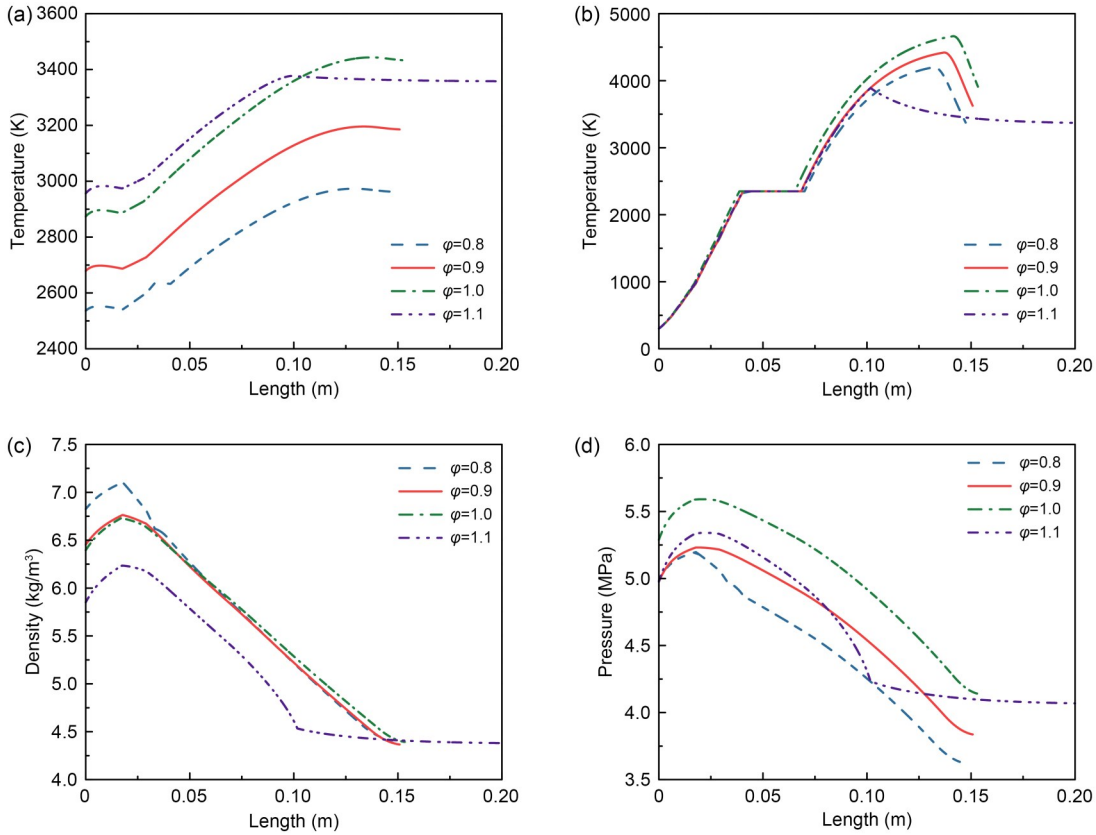

Fig. 10 Distribution of the detonation wave flow field parameters under different reaction equivalence ratios: (a) gas phase temperature; (b) particle phase temperature; (c) gas phase density; (d) detonation pressure

absorb heat. As shown in Fig. 10a, the gas phase temperature in the front section of the detonation wave flow field increases with the increase of the equivalence ratio. This is because the increase of the equivalence ratio causes a relative decrease in the amount of incoming lower-temperature air. With the progress of the chemical reaction, the release of heat undermines the influence of incoming air, and the gas phase temperature finally reaches the peak value at the stoichiometric ratio. As shown in Fig. 10c, the gas phase density in the front section of the detonation wave flow field decreases as the equivalence ratio increases, which is because the increase of the equivalence ratio reduces the mass of the gas phase. With the progress of the reaction, the gas phase density at the CJ plane reaches the peak value at the stoichiometric ratio.

4 Conclusions

In this study, a 1D steady-state detonation wave model of boron-based gel propellant was established. The model considered the diverse heterogeneous chemical reaction processes occurring in the induction and reaction regions, as well as the implications of pressure variations and the latent heat associated with phase transitions on these reactions. The model was validated by comparing the peak pressures of the detonation wave obtained by numerical simulations and ground tests. The results show that the peak pressure of the detonation wave can reach 6.15 MPa, and the model exhibits a maximum deviation of 8%.

Upon iterative calculations, the eigenvalue detonation velocity of a boron-based gel propellant under default working conditions was obtained as 1831.5 m/s. The effects of incoming flow conditions, propellant parameters, and the initial operating state on the detonation wave flow field of the propellant were analyzed by numerical simulation. The results revealed that the stable and self-sustaining propagation of the detonation wave can be achieved only when its propagation velocity matches the eigenvalue detonation velocity. As the incoming flow temperature rises, there is a corresponding decrease in the gas phase temperature,

particle phase temperature, gas phase density, and pressure within the steadily propagating detonation wave. With the increase of the boron content of the gel propellant, there is a notable rise in the gas phase temperature, gas phase density, and pressure at the CJ plane. In addition, as the reaction equivalence ratio increases, the gas phase temperature, particle phase temperature, gas phase density, and pressure increase first and then decrease, peaking at the stoichiometric ratio. These conclusions have significance for guiding the application of boron-based gel propellants for detonation. In future research, detailed chemical reaction mechanisms and more accurate ignition and combustion models for boron particles will be used to further improve the accuracy of the calculation results.

Acknowledgments

This work is supported by the Science and Technology Innovation Program of Hunan Province (No. 2022RC3045), the Hunan Provincial Natural Science Foundation of China (No. 2023JJ30635), and the National Natural Science Foundation of China (No. 12302394).

Author contributions

He YANG and Liya HUANG designed the research. Jiarui ZHANG, Kun LIANG, and Mingquan GONG processed the corresponding data. He YANG wrote the first draft of the manuscript. Liya HUANG and Jiarui ZHANG helped to organize the manuscript. All authors revised and edited the final version.

Conflict of interest

He YANG, Liya HUANG, Jiarui ZHANG, Kun LIANG, and Mingquan GONG declare that they have no conflict of interest.

References

Chen W, Zhang MZ, 2011. The current status and future prospects of gel propellants. The 5th National Conference on Chemical Propellant (in Chinese).

Duan L, Xia ZX, Feng YC, et al., 2023. Effect of carbon dioxide concentration on the combustion characteristics of boron agglomerates in oxygen-containing atmospheres. *Journal of Zhejiang University-SCIENCE A*, 24(11):949-959. https://doi.org/10.1631/jzus.A2200468

Fan WJ, Zhou J, Liu SJ, et al., 2021. Effects of the geometrical parameters of the injection nozzle on ethylene-air continuous rotating detonation. *Journal of Zhejiang University-SCIENCE A*, 22(7):547-563. https://doi.org/10.1631/jzus.A2000314

Fan WJ, Liu WD, Peng HY, et al., 2022. Numerical study on ethylene-air continuous rotating detonation in annular combustors with different widths. *Journal of Zhejiang University-SCIENCE A*, 23(5):388-404. https://doi.org/10.1631/jzus.A2100448

Foelsche RO, Burton RL, Krier H, 1999. Boron particle ignition and combustion at 30-150 atm. *Combustion and Flame*, 117(1-2):32-58. https://doi.org/10.1016/s0010-2180(98)00080-7

Glushkov DO, Paushkina KK, Pleshko AO, et al., 2023. Ignition and combustion behavior of gel fuel particles with metal and non-metal additives. *Acta Astronautica*, 202:637-652. https://doi.org/10.1016/j.actaastro.2022.11.027

Han JX, Bai QD, Zhang SJ, et al., 2022. Experimental study on propagation characteristics of rotating detonation wave with kerosene fuel-rich gas. *Defence Technology*, 18(8):1498-1512. https://doi.org/10.1016/j.dt.2022.04.004

Hong T, Qin CS, Lin WZ, 2009. Numerical simulation of detonation in suspended mixed RDX and aluminum dust. *Explosion and Shock Waves*, 29(5):468-473 (in Chinese). https://doi.org/10.11883/1001-1455(2009)05-0468-06

Hu HB, Weng CS, 2011. One dimensional numerical calculation for influence of aluminum concentration on multiphase detonation of suspended gasoline/nano-aluminum-powder liquid drops. *Journal of Rocket Propulsion*, 37(5):47-51 (in Chinese). https://doi.org/10.3969/j.issn.1672-9374.2011.05.009

Hu HB, Weng CS, 2016. Transient characteristics for working process of pulse detonation engine with aluminized gelled fuels. *Journal of Solid Rocket Technology*, 39(4):463-469 (in Chinese). https://doi.org/10.7673/j.issn.1006-2793.2016.04.003

Huang LY, Gong MQ, Zhang JR, et al., 2024. High-energy-density metallized gel propellant by hydrogen-bonded polymer-small molecules for enhanced stability and shear-thinning performance. *Acta Astronautica*, 214:356-365. https://doi.org/10.1016/j.actaastro.2023.10.047

Jin YS, Xu X, Yang QC, et al., 2022. Combustion behavior of hydrocarbon/boron gel-fueled scramjet. *AIAA Journal*, 60(6):3834-3843. https://doi.org/10.2514/1.J061326

King MK, 1972. Boron ignition and combustion in air-augmented rocket afterburners. *Combustion Science and Technology*, 5(1):155-164. https://doi.org/10.1080/00102207208952516

Küçükosman R, Değirmenci H, Yontar AA, et al., 2023. Combustion characteristics of gasoline fuel droplets containing boron-based particles. *Combustion and Flame*, 255:112887. https://doi.org/10.1016/j.combustflame.2023.112887

Lei ZD, Chen ZW, Yang XQ, et al., 2020. Operational mode transition in a rotating detonation engine. *Journal of Zhejiang University-SCIENCE A*, 21(9):721-733. https://doi.org/10.1631/jzus.A1900349

Li JL, Fan W, Yan CJ, et al., 2009. Experimental investigations on detonation initiation in a kerosene-oxygen pulse detonation rocket engine. *Combustion Science and Technology*, 181(3):417-432. https://doi.org/10.1080/00102200802612310

Li JL, Fan W, Yan CJ, et al., 2011. Performance enhancement

of a pulse detonation rocket engine. *Proceedings of the Combustion Institute*, 33(2):2243-2254. https://doi.org/10.1016/j.proci.2010.07.048

Li SC, Williams FA, 1991. Ignition and combustion of boron in wet and dry atmospheres. *Symposium (International) on Combustion*, 23(1):1147-1154. https://doi.org/10.1016/s0082-0784(06)80374-7

Liang K, Huang LY, Zhang JR, et al., 2024. Experimental investigation on detonation characteristics of boron-rich gelled propellant in static premixed combustible gases. *Acta Astronautica*, 220:263-273. https://doi.org/10.1016/j.actaastro.2024.04.036

Liang X, Wang RL, 2019. Verification and validation of detonation modeling. *Defence Technology*, 15(3):398-408. https://doi.org/10.1016/j.dt.2018.11.005

Liu JD, Xiao W, Dai J, 2024. The influence of supersonic spatial-temporal coupling disturbance on detonation in an expanded chamber. *Aerospace Science and Technology*, 147:109024. https://doi.org/10.1016/j.ast.2024.109024

Liu L, Xia ZX, Huang LY, et al., 2020. Numerical investigation of one-dimensional unsteady detonation wave characteristics of magnesium particle-air mixture. *Acta Physica Sinica*, 69(19):194701 (in Chinese). https://doi.org/10.7498/aps.69.20200549

Liu WD, Peng HY, Liu SJ, et al., 2023. Research progresses of rotating detonation combustion and its application. *Acta Aeronautica et Astronautica Sinica*, 44(15):528875 (in Chinese). https://doi.org/10.7527/S1000-6893.2023.28875

Lu XY, Kaplan CR, Oran ES, 2021. A chemical-diffusive model for simulating detonative combustion with constrained detonation cell sizes. *Combustion and Flame*, 230:111417. https://doi.org/10.1016/j.combustflame.2021.111417

Meng HL, Xiao Q, Feng WK, et al., 2022. Air-breathing rotating detonation fueled by liquid kerosene in cavity-based annular combustor. *Aerospace Science and Technology*, 122:107407. https://doi.org/10.1016/j.ast.2022.107407

Miao SK, Zhou J, Liu Y, et al., 2019. Review of studies on oblique detonation waves in supersonic flows. *Journal of Experiments in Fluid Mechanics*, 33(1):41-53 (in Chinese). https://doi.org/10.11729/syltlx20180078

Nachmoni G, Natan B, 2000. Combustion characteristics of gel fuels. *Combustion Science and Technology*, 156(1):139-157. https://doi.org/10.1080/00102200008947300

Padwal MB, Natan B, Mishra DP, 2021. Gel propellants. *Progress in Energy and Combustion Science*, 83:100885. https://doi.org/10.1016/j.pecs.2020.100885

Palaszewski B, Jurns J, Breisacher K, et al., 2004. Metallized gelled propellants combustion experiments in a pulse detonation engine. The 40th AIAA/ASME/SAE/ASEE Joint Propulsion Conference and Exhibit. https://doi.org/10.2514/6.2004-4191

Pang WQ, Yetter RA, Deluca LT, et al., 2022. Boron-based composite energetic materials (B-CEMs): preparation, combustion and applications. *Progress in Energy and Combustion Science*, 93:101038. https://doi.org/10.1016/j.pecs.2022.101038

Rojas Chavez SB, Chatelain KP, Lacoste DA, 2023. Two-dimensional visualization of induction zone in hydrogen detonations. *Combustion and Flame*, 255:112905. https://doi.org/10.1016/j.combustflame.2023.112905

Salvadori M, Panchal A, Menon S, 2023. Simulation of liquid droplets combustion in a rotating detonation engine. *Proceedings of the Combustion Institute*, 39(3):3063-3072. https://doi.org/10.1016/j.proci.2022.09.002

Schumaker SA, Knisely AM, Hoke JL, et al., 2021. Methane–oxygen detonation characteristics at elevated pre-detonation pressures. *Proceedings of the Combustion Institute*, 38(3):3623-3632. https://doi.org/10.1016/j.proci.2020.07.066

Shao YT, Liu M, Wang JP, 2010. Numerical investigation of rotating detonation engine propulsive performance. *Combustion Science and Technology*, 182(11-12):1586-1597. https://doi.org/10.1080/00102202.2010.497316

Shen DW, Ma JZ, Sheng ZH, et al., 2022. Spinning pulsed detonation in rotating detonation engine. *Aerospace Science and Technology*, 126:107661. https://doi.org/10.1016/j.ast.2022.107661

Sun HJ, Zhang HB, Bai BF, 2008. Evaporation investigation of single droplet in high temperature fuel gas. *Journal of Xi'an Jiaotong University*, 42(7):833-837 (in Chinese). https://doi.org/10.3321/j.issn:0253-987X.2008.07.011

Sun ZP, Huang Y, Luan ZY, et al., 2023. Three-dimensional simulation of a rotating detonation engine in ammonia/hydrogen mixtures and oxygen-enriched air. *International Journal of Hydrogen Energy*, 48(12):4891-4905. https://doi.org/10.1016/j.ijhydene.2022.11.029

von Kampen J, Alberio F, Ciezki HK, 2007. Spray and combustion characteristics of aluminized gelled fuels with an impinging jet injector. *Aerospace Science and Technology*, 11(1):77-83. https://doi.org/10.1016/j.ast.2006.08.006

Wang F, Weng CS, 2022. Numerical research on two-phase kerosene/air rotating detonation engines. *Acta Astronautica*, 192:199-209. https://doi.org/10.1016/j.actaastro.2021.12.026

Wang ZG, Liang JH, Ding M, et al., 2009. A review on hypersonic airbreathing propulsion system. *Advances in Mechanics*, 39(6):716-739 (in Chinese). https://doi.org/10.6052/1000-0992-2009-6-J2008-126

Yang DL, Xia ZX, Huang LY, et al., 2018. Exprimental study on the evaporation characteristics of the kerosene gel droplet. *Experimental Thermal and Fluid Science*, 93:171-177. https://doi.org/10.1016/j.expthermflusci.2017.12.031

Yuan JF, Liu JZ, Zhang LQ, et al., 2021. Combustion and agglomeration characteristics of boron particles in boron-containing fuel-rich propellant. *Combustion and Flame*, 232:111551. https://doi.org/10.1016/j.combustflame.2021.111551

Zhou JH, Liu JZ, Zhang YW, et al., 2015. Ignition and Combustion of Boron. Science Press, Beijing, China (in Chinese).